ACS APPLIED MATERIALS & INTERFACES

Research Article

www.acsami.org

Effect of Ion-Chelating Chain Lengths in Thiophene-Based Monomers on in Situ Photoelectrochemical Polymerization and Photovoltaic Performances

In Young Song, Minjun Kim, and Taiho Park*

Department of Chemical Engineering, Pohang University of Science and Technology, San31, Nam-gu, Pohang, Kyoungbuk 790-780, Korea

Supporting Information

ABSTRACT: We synthesized thiophene-based monomers (bis-EDOTs) with different ethylene glycol oligomer (EGO) lengths (TBO3, TBO4, and TBO5) and investigated their polymerization characteristics during photoelectrochemical polymerization (PEP) at the surfaces of dye (D205)-sensitized TiO_2 nanocrystalline particles. During the PEP reaction, monomers were expected to diffuse toward neighboring dyes through the growing polymer layers to enable continuous chain growth. We found that the less bulky monomer (TBO3) formed a more compact polymer layer with a high molecular weight. Its diffusion to the active sites through the resulting growing polymer layer was, therefore, limited. We deployed layers of the polymers (PTBO3, PTBO4, and PTBO5) in iodine-free solid-state hybrid solar cells to investigate the lithium ion chelating properties of the polymers as a function of the number of oxygen atoms present in the EGOs. PTBO4 and PTBO5 were capable of chelating lithium ions, yielding a photovoltaic performance that was 142% of the performance obtained without the polymer layers (3.0 → 5.2%).

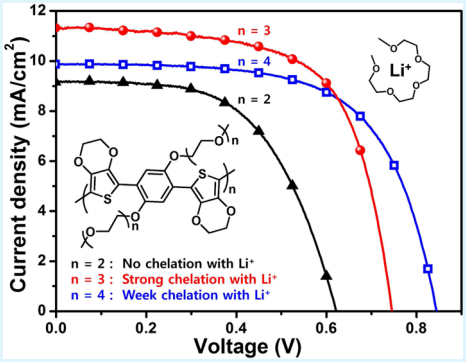

KEYWORDS: *ion-chelating, thiophene-based monomers, charge transport, photoelectrochemical polymerization, photovoltaic performances*

INTRODUCTION

Conducting polymers based on fused heteroaromatic moieties, including sulfur, nitrogen, oxygen, or selenium, are widely employed in a variety of photocells and organic field effect transistors due to their excellent optoelectronic properties.[1−7] These polymers may be prepared via metal-mediated condensation polymerization reactions involving functionalized monomers.[8−13] Meanwhile, photoelectrochemical polymerization (PEP) can be applied to monomers without functional groups. Without catalysts, an active radical species can be directly generated on the sp^2 carbon of ends of the growing polymer, which then undergo coupling reactions with new monomers.[14−16] For example, Yanagida reported the in situ PEP of pyrroles and bis-EDOT as a hole-transporting material (HTM) to replace the I^-/I_3^- solution in an iodine-free solid-state DSSC (s-DSSC).[17] They reported a 2.85% power conversion efficiency (PCE). Ramakrishna,[18] Hagfeldt,[19] Jouini,[20] Liu,[21] and Han[22] independently deployed this approach in solar cells because the in situ PEP provides an effective means for filling the nanosize pore spaces within the TiO_2 electrodes using the resulting conducting polymer. We reported the in situ PEP of a novel PEDOT derivative (TBO4) having tetraethylene glycol (TEG) side chains, which strongly chelate lithium ions (Li^+), to improve the power conversion efficiency (η = 1.6 → 2.9%).[23] We reported the preparation of a highly insoluble all-conducting block copolymer (PEDOT-*b*-PTBO4) using the in situ PEP.[24] This block polymer encapsulated nanocrystalline dyed TiO_2 particles, resulting in the formation of a block copolymer bilayer hybrid nanostructure. We selectively positioned lithium ions on the PTBO4 layer to realize highly efficient charge collection (95%, η = 6.5%) in the solar cell.

During the preparation of the well-defined block copolymers, we found that the sequential order of the monomer addition was important for obtaining the block copolymers. Here, we synthesized two novel bis-EDOT derivatives having different ethylene glycol oligomer (EGO) side chain lengths (TBO3 and TBO4) to clarify the in situ PEP mechanism, as shown in Scheme 1. It is unclear whether the superior photovoltaic performances of the TBO4 prepared with the TEG side chains, relative to the bis-EDOT without the EGO side chains, resulted from the flexibility of the chains or from the Li^+-chelating ability.

The in situ PEP is understood as being initiated by holes generated on the HOMO level of the dye after the sensitizer has been excited by light (see Figure S1, Supporting Information, for the detailed polymerization mechanism).[18] The oxidized dye is neutralized by electron transport from a

Received: March 20, 2015
Accepted: May 15, 2015
Published: May 15, 2015

DOI: 10.1021/acsami.5b02411
ACS Appl. Mater. Interfaces 2015, 7, 11482−11489

Scheme 1. Synthetic Routes to Monomers (TBO3, n = 3; TBO4, n = 4; and TBO5, n = 5) and Corresponding Polymers (PTBO3, PTBO4, and PTBO5) Prepared Using the in Situ Photoelectrochemical Polymerization (PEP) Method[a]

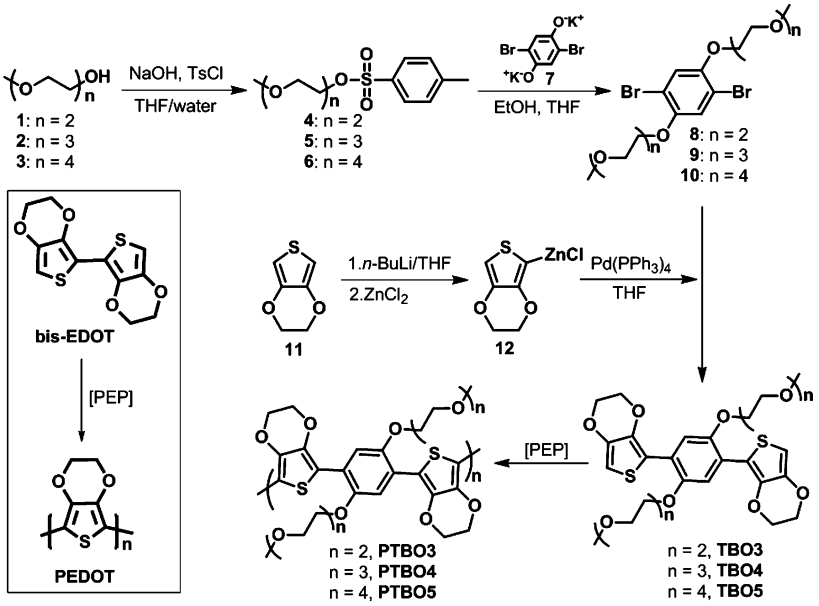

[a]Structures of the bis-EDOT and PEDOT are also shown. See Supporting Information for the detailed synthesis and characterization of the monomers.

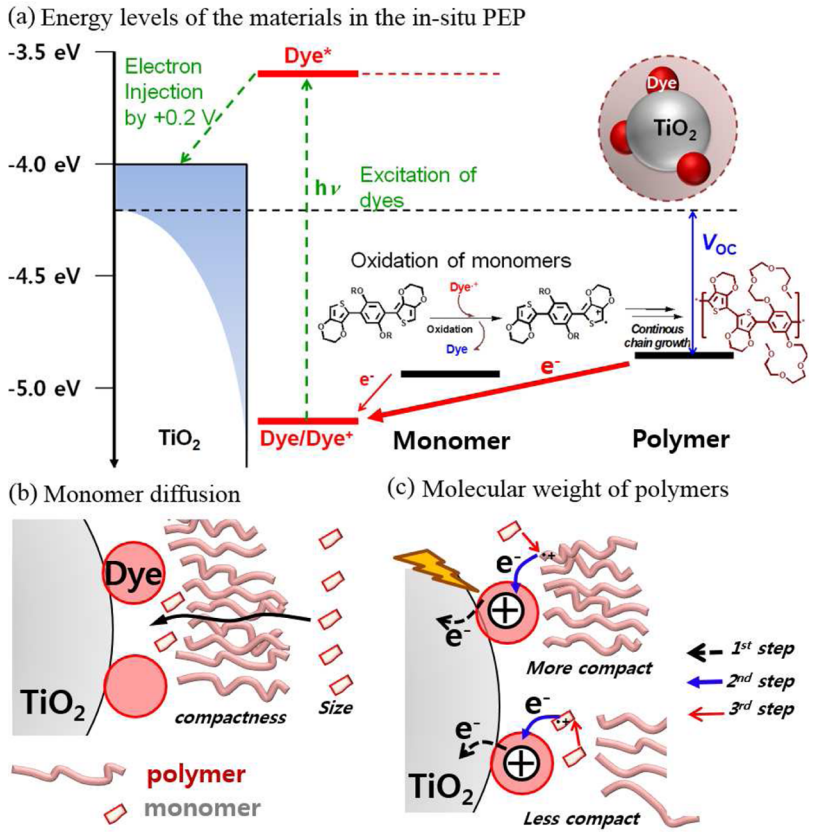

Figure 1. (a) Relative energy levels of the monomer and the resulting polymer. Electron transport from the end of the polymer was dominant over electron transport from the monomer during neutralization of an oxidized dye because the polymer was more easily oxidized than the monomer.[23−26] (b) Illustration of monomer diffusion through the growing polymers, and (c) the effects of polymer layer compactness on the chain growth. Neutralization of an oxidized dye via electron transport from either an end of a growing polymer chain or a monomer, depending on the compactness of the growing polymer layer, affording high or low molecular weights, respectively.

DOI: 10.1021/acsami.5b02411
ACS Appl. Mater. Interfaces 2015, 7, 11482−11489

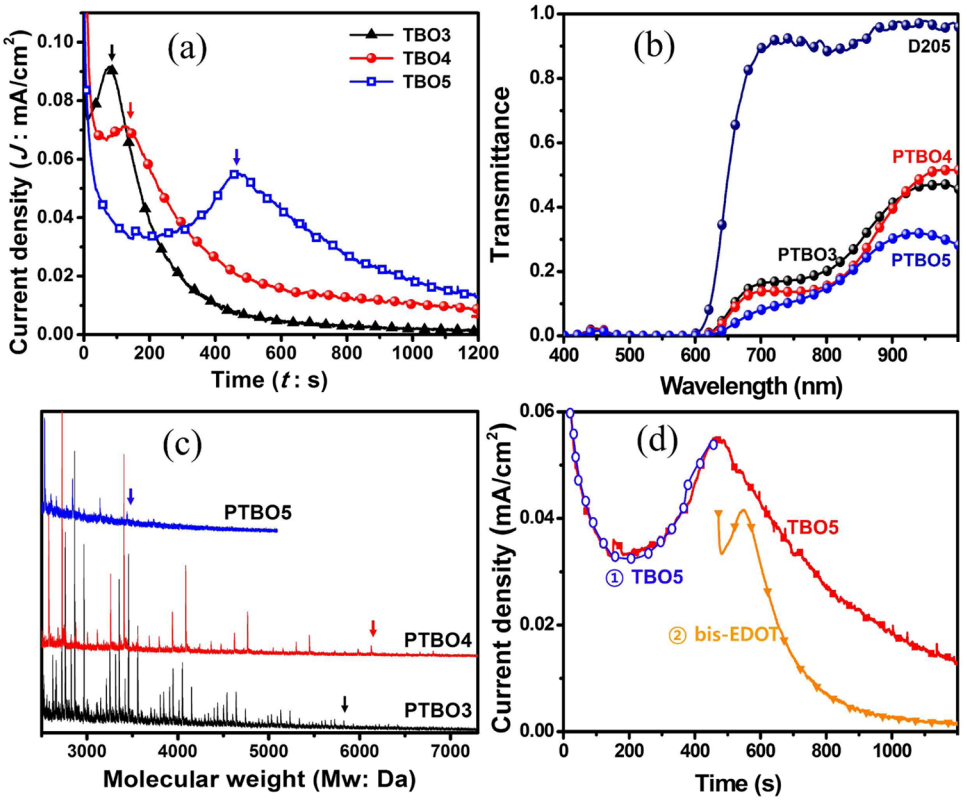

Figure 2. (a) Current density–time (J–t) curves obtained during the in situ PEP of TBO3, TBO4, and TBO5 (0.01 M monomers in a 0.1 M LiTFSI solution (acetonitrile), illumination at λ > 520 nm, +0.2 V). (b) The transmittance spectra of the D205-sensitized photoanodes in the absence or presence of the polymer layers. (c) Solvent-less MALDI-TOF MS spectra of PTBO3, PTBO4, and PTBO5 (polymerization time: 20 min). The ground polymer-coated TiO_2 particles were mixed with a 2,5-dihydroxybenzoic acid matrix. The mixture was then smeared onto the substrate to measure the solvent-less MALDI-TOF MS spectrum. (d) A comparison of the sequential in situ PEP curve obtained from TBO5, followed by bis-EDOT, with an in situ PEP of TBO5.

growing polymer because the highest occupied molecular orbital (HOMO) level of the growing polymer should exceed that of the dye due to the extend conjugation. A coupling reaction between the resulting oxidized polymer and a new monomer may further advance the growth of the polymer (Figure 1a). New monomers should, therefore, diffuse to the space through the growing polymer layer (Figure 1b). The ability of the monomers to penetrate the growing polymer layer may depend on either the compactness of the growing polymer layer or the bulkiness of the monomers. The compactness of the polymer layer could alter the distance between the dye and the end of the polymer, which can also affect the polymer molecular weight. For example, it is possible that if a polymer end is far from an oxidized dye molecule (for example, in a less compact layer such as the one shown in Figure 1c), the dye molecule may be neutralized by a monomer neighboring the dye. The resulting oxidized monomer could then be coupled to a new monomer. This dominant process may result in a low polymer molecular weight.

Here, we report the interplay between the monomer bulkiness and the polymer layer compactness during an in situ PEP using thiophene-based monomers with various EGO side chain lengths (Scheme 1). We also report the effects of the Li^+ chelation properties on the photovoltaic performances in the iodine-free solid-state hybrid solar cells (DSCs).

RESULTS AND DISCUSSION

The in situ PEP of three monomers, TBO3, TBO4, and TBO5, was carried out to obtain the corresponding polymers with encapsulation of dye-coated nanocrystalline TiO_2 electrodes (denoted PTBO3, PTBO4, and PTBO5, respectively). The current density (J) profiles versus the in situ PEP time (J–t curves) were monitored using cyclic voltammetry (Figure 2a) and their results are summarized in Table 1. All monomers exhibited an exponential decay of J_s after their J values had reached a maximum (J_{max}, marked with arrows in Figure 2a). The J_{max} value for TBO5 appeared at 481 s, much longer than the values obtained from TBO3 and TBO4 (94 and 118 s, respectively). The integrated area under the J–t curves is equivalent to the quantity of charge (Q), which is proportional to the polymerization by the diffused monomers. This is related

Table 1. Summary of Binding Constants of TBO3, TBO4, and TBO5 and the Results Obtained from Their in Situ Photoelectrochemical Polymerization (PEP)

polymers	size of monomers	time at J_{max} (s)	Q^a (mC/cm²)	M_w	$K_a{}^b$ (M^{-1})
PTBO3	smallest	94	22	5800	
PTBO4	middle	118	34	6200	495
PTBO5	largest	481	41	3750	239

[a]The charge transported during the in situ PEP, calculated by multiplying the current density and the PEP time. [b]Binding constant for the 1:1 complexation mode (see the Supporting Information).

DOI: 10.1021/acsami.5b02411
ACS Appl. Mater. Interfaces 2015, 7, 11482–11489

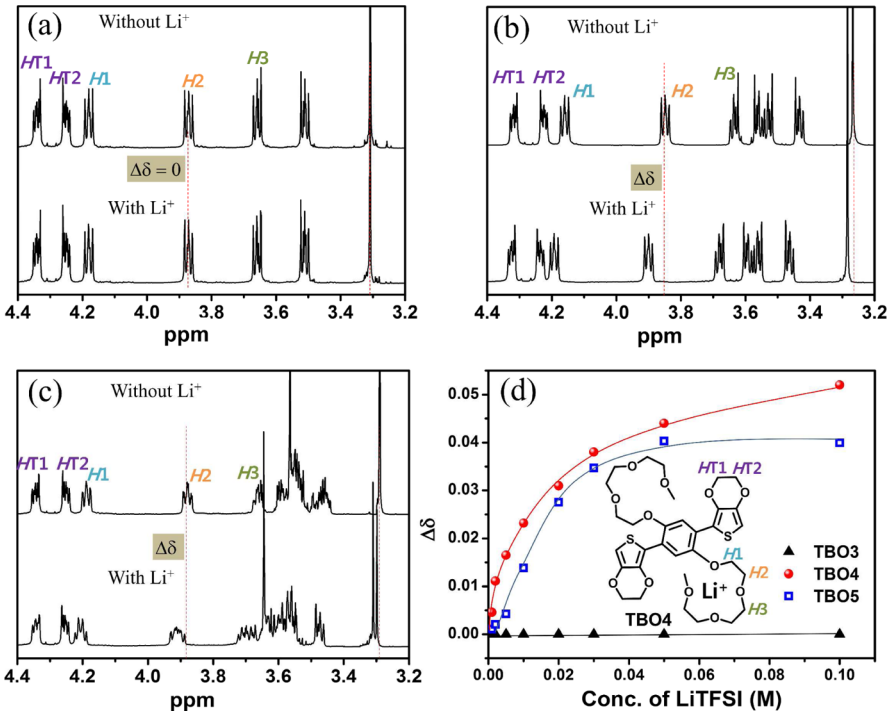

Figure 3. (a–c) Representative ^{1}H NMR spectra of TBO3, TBO4, and TBO5 before and after the addition of LiTFSI. (d) Plots of $\Delta\delta$ (chemical shifts of H2) versus concentrations of LiTFSI (0.01 M of monomers).

to the quantity of the polymer (either the number of chains or the degree of polymerization).[23,24] These results indicated that the diffusion of TBO5 toward the active sites (between the neighboring dye-coated TiO_2 nanoparticles) through the growing polymer layer was easier than the diffusion of TBO3 and TBO4. The quantity of the PTBO5 polymer produced from the in situ PEP was much greater than the quantities of TBO3 and TBO4, as estimated from the magnitudes of the charges transported (Q = 22, 34, and 41 mC/cm^2 for TBO3, TBO4, and TBO5, respectively). These results were confirmed by the transmittance spectra obtained from the resulting polymer films (Figure 2b). The transmittance of PTBO5 was much lower than the corresponding values of PTBO3 and PTBO4 beyond 630 nm.

As mentioned above, a high polymer M_w could be achieved by ensuring that electron transport (oxidation) during oxidized dye neutralization proceeded from the end of the growing polymer to the oxidized dye. This process was favorable because the polymers were more easily oxidized than the corresponding monomers (Figure 1a).[23−26] Electron transport from the polymers to the oxidized dyes dominated the corresponding monomers, although the monomers were closer to the oxidized dye. The production of a low molecular weight (M_w) polymer, therefore, indicated the presence of two effects: (1) the distance between the polymer end and the oxidized dye was too long to permit electron transport from the polymer to the oxidized dye; and (2) a large separation between polymer chains formed a less compact polymer layer, which did not limit monomer diffusion to the oxidized dye. This case is expected from the in situ PEP of a more bulky monomer (e.g., TBO5). Indeed, the M_w of PTBO5, which was estimated using solventless matrix-assisted laser desorption ionization-time-of-flight mass spectrometry (MALDI-TOF MS)[27] due to the insolubility of the polymer in most organic solvents, was 3750 Da. This value was 2000 Da smaller than the value obtained from TBO3 (Figure 2c), indicating that it was difficult for TBO5 to participate on the coupling reaction with the growing polymer toward a high M_w, although the in situ PEP of TBO5 produced larger numbers of the polymer chains (PTBO5) due to the less hindered diffusion through the resulting polymer (PTBO5) layer. In turn, the smaller monomer TBO3 produced a more compact polymer (PTBO3) layer that more tightly encapsulated the dye-coated TiO_2 nanoparticles. We concluded that the compactness of polymer layer was the dominant factor to determine the molecular weight of the polymer during the in situ PEP. The in situ sequential polymerization of TBO5, followed by bis-EDOT (① → ② in Figure 2d) also supported our conclusion. The smallest monomer bis-EDOT did not undergo a better PEP process through the less compact PTBO5 layer because bis-EDOT suddenly formed a highly compact polymer layer (PEDOT) (see Figure S2, Supporting Information, for the illustrated polymerization process).

The chelation properties (binding constant, K_a) of the three monomers (TBO3, TBO4, and TBO5) with Li^+ ions were investigated using ^{1}H NMR spectroscopy.[28−30] Unlike TBO3 (Figure 3a), the proton peaks corresponding to the EGOs in TBO4 and TBO5 were shifted toward higher ppm values (Figure 3b,c) as the concentration of LiTFSI increased (0.001−0.1 M) in a d-acetonitrile solution of the individual monomers (0.01 M). These results were fit to an association model, giving K_a = 495 and 239 M^{-1}, respectively (Figure 3d) (see the Supporting Information for a detailed description of the model).[31] These results demonstrated that the EGOs with four oxygen atoms (TBO4) more strongly associated with the Li^+ ions than did the EGOs with five oxygen atoms (TBO5).

A computational study of the complexes TBO4:2Li^+ and TBO5:2Li^+ was performed to deepen our understanding of the observed differences in the binding properties using density functional theory (DFT) and the Gaussian 03 package at the B3LYP/6-31+G* level of theory (Figure 4).[32] The weak

DOI: 10.1021/acsami.5b02411
ACS Appl. Mater. Interfaces 2015, 7, 11482−11489

association between TBO5 and Li^+ was ascribed to the distorted geometry due to the presence of more bulky side chains.

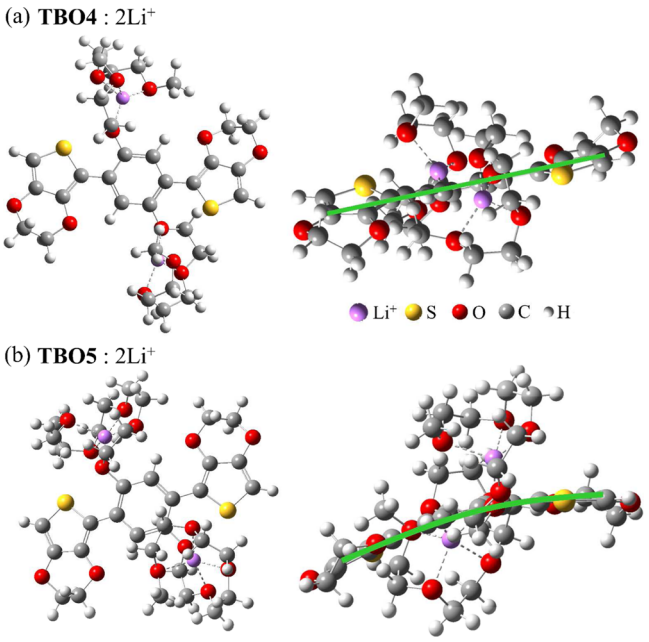

Figure 4. Top and side views of complexes (a) TBO4:2Li^+ and (b) TBO5:2Li^+ estimated using density functional theory (DFT) and the Gaussian 03 package at the B3LYP/6-31+G* level of theory.

Photovoltaic performances of the various polymers were evaluated in iodine-free dye-sensitized solar cells,[17,33] and the obtained parameters are summarized in Table 2 (see Figure S3, Supporting Information, for the reproducibility of the devices). The addition of Li^+ to an aprotic electrolyte shifted the band edge away from the vacuum level (producing lower-lying quasi-Fermi levels) in the TiO_2 electrode due to the adsorption of Li^+ onto the polar surfaces of the TiO_2 particles (Figure 5).[34,35] This effect decreased the open circuit voltage (V_{OC}) as a theoretical V_{OC} was determined by the energy difference between the quasi-Fermi level of the nanocrystalline TiO_2 electrode under illumination and the redox level of the HTM.[36−39] Furthermore, the photoinduced electrons [$e^-(TiO_2)$] relaxed to the lowest energy level of the conduction band (CB) and were subsequently trapped in the intraband states of the surface.[40,41] The electrons in the trap states could then recombine with the cationic dyes (R_1) or the cationic HTMs (R_2). These process also decreased V_{OC} as well as J_{SC}.[42−46] It should be noted that R_2 dominated R_1 because hole transport from the dye to the HTM was efficient.

Table 2. Parameters Related to the in Situ PEP and Intrinsic Properties of the Resulting Polymers

	J_{SC} (mA/cm^2)	V_{OC} (V)	FF	PCE (%)	τ_{trans} (ms)^a	τ_{rec} (ms)^b	η (%)^c
PTBO3	9.1	0.62	53.3	3.0	2.5	9.1	72
PTBO4	11.4	0.75	60.0	5.1	1.8	10.9	83
PTBO5	9.8	0.83	63.7	5.2	1.6	16.7	90

^{a}Electron transport time. ^{b}Electron recombination time. ^{c}Charge collection efficiency calculated from η (%) = [1 − (τ_{trans}/τ_{rec})]100.

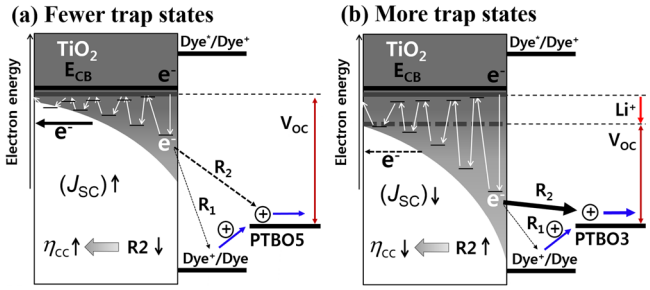

Figure 5. Illustration of the competitive reactions that occurred at the dye/TiO_2/polymeric HTM interface; (a) fewer trap states in PTBO5 and (b) more trap states in PTBO3.

Indeed, we obtained low values of V_{OC} (0.62 V), J_{SC} (9.1 mA/cm^2), and FF (53.3), with a PCE of 3.0%, in the device prepared using PTBO3 (Figure 6a) because PTBO3 could not prevent the adsorption of Li^+ into TiO_2. These effects were in good agreement with our previous results, obtained from the bis-EDOT monomer, which did not include Li^+ chelating side chains.[23] PTBO4, which had strong Li^+ chelating properties, provided an improved PCE of 5.1% with simultaneously improved V_{OC} (0.75 V) and J_{SC} values (11.4 mA/cm^2). These effects arose because Li^+ ions were not permitted to adsorb onto the polar surface of the TiO_2. In addition, Li^+ ions were well incorporated into the matrix of the PTBO4 layer, thereby facilitating hole transport to the counter electrode (reducing recombination), as indicated by the improved FF value (53.3 → 60.0). Interestingly, the V_{OC} of the device prepared using PTBO5 was 0.83 V, better than the value obtained from the device prepared using PTBO4, 0.75 V, but the J_{SC} value decreased from 11.4 (for the PTBO4 device) to 9.9 mA/cm^2 (for the PTBO4 device). As discussed above, the larger value of Q obtained from PTBO5 exceeded the value obtained from PTBO4; thus, PTBO5 may have bound more Li^+ ions, although its binding capacity was slightly lower than that of PTBO4. The large quantity of PTBO5 partially occluded light harvesting, as indicated by the transmittance spectra (Figure 2c), which decreased J_{SC}.

We measured impedance by using EIS, and we have reconfigured the results to Nyquist and Bode plots to determine the recombination resistance and lifetime of polymers, respectively.[47,48] The small semicircle measured at high frequencies and the larger semicircle at low frequencies (in the dark) in the Nyquist plots were attributed to the charge transfer at the polymer/Ag counter electrode and electron recombination at the TiO_2/the polymer interface, respectively.[49,50] The recombination resistance (R_{rec}) values between the TiO_2 layer and the polymer were ordered according to increasing value: PTBO3 (125 Ω), PTBO4 (220 Ω), and PTBO5 (425 Ω). The electron lifetimes (τ_n), estimated from the Bode phase plots, increased in the order of PTBO3 (12.8 ms), PTBO4 (13.6 ms), and PTBO5 (15.3 ms). These results indicated that PTBO5 bound more Li^+ ions, and thus, lower quantities of Li^+ ions were adsorbed onto the polar surfaces of the TiO_2 particles. We collected the intensity-modulated photocurrent/photovoltage spectra (IMPS/IMVS) to measure the charge collection efficiency[51−54] ($\eta_{cc} \approx 1 - (\tau_{trans}/\tau_{rec})$, where τ_{trans} is the electron transport time, and τ_{rec} is the recombination time, see Supporting Information for details), as shown in Figure 6d. The value of τ_{trans} decreased in the order of TBO3 (2.5 ms), TBO4 (1.8 ms), and TBO5 (1.6 ms) but τ_{rec} increased in the order of TBO3 (9.1 ms), TBO4 (10.9 ms), and

DOI: 10.1021/acsami.5b02411
ACS Appl. Mater. Interfaces 2015, 7, 11482−11489

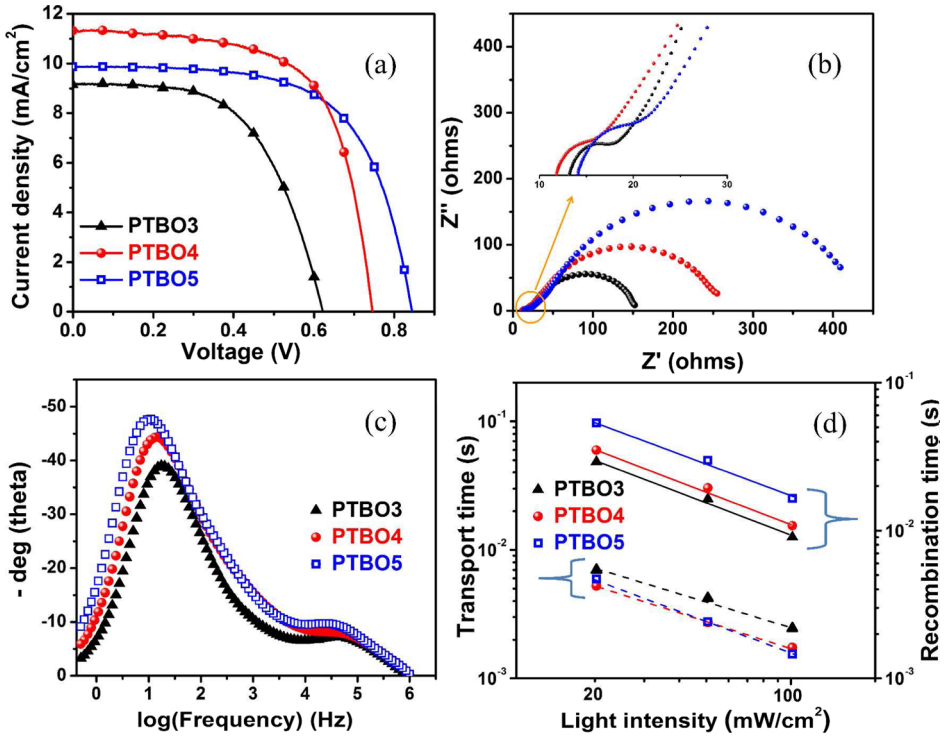

Figure 6. (a) Current density−voltage curves of the devices prepared using PTBO3, PTBO4, or PTBO5. (b) Nyquist and (c) Bode phase plots obtained from the electrochemical impedance spectra (EIS) measured at −0.69 V in the dark. (d) IMPS/IMVS spectra used to estimate the charge collection efficiencies of the devices.

TBO5 (16.7 ms), indicating that fewer trap states were present on the TiO_2 particle surfaces due to the low adsorption of Li^+ ions on the TiO_2 particle surfaces. The η_{cc} value obtained from PTBO5 was 90%, which was greater than that (83%) obtained from PTBO4 (Table 2).

The low value of η_{cc} for PTBO4 was ascribed to the low conductivity (e.g., inefficient hole transport to the counter electrode). In general, the conductivity was influenced by the M_w of the polymer matrix in the presence of the proper amounts of Li^+. For example, as reported by Snaith,[55] an excess of Li^+ ions decreased the conductivity. The conductivity of PTBO3 (M_w = 5800 Da), measured using the 4-point probe method, was 62 S/cm, which exceeded the value obtained from PEDOT (34 S/cm), which had a similar M_w (6000 Da). This value was even greater than the values obtained from PTBO5 (40 S/cm) and PTBO4 (55 S/cm), indicating that a certain quantity of Li^+ ions was incorporated into the PTBO3 matrix, although strong Li^+ chelation was not present. An excess of Li^+ ions bound to PTBO4 and PTBO5 due to the chelating properties of these Li^+ ions. The weak binding properties of PTBO3, in turn, led the adsorption of the largest quantity of Li^+ ions onto the polar surfaces of the TiO_2 particles, which increased the number of trap states.

CONCLUSION

We concluded that different numbers of oxygen atoms present on the monomer side chains influenced their in situ PEP processes, their Li^+ ion chelation strength, and the photovoltaic performances of the iodine-free DSCs. We demonstrated that a monomer having 4 or more oxygen atoms on the side chain could strongly chelate Li^+ ions. This binding process minimized the adsorption of Li^+ ions on the polar surfaces of the TiO_2 particles, thereby improving the electron extraction/collection processes. This work has provided a deep understanding of the charge transport mechanisms that operate at heterogeneous interfaces, as well as the relationship between material design and device function.

ASSOCIATED CONTENT

Supporting Information

Experimental details; calculation of the binding constant of TEG-Li^+ complexes; detailed in situ PEP mechanism, sequential in situ PEP curve obtained from TBO5, followed by bis-EDOT and illustration of the process; reproducibility of the photovoltaic parameters obtained by 5 devices.The Supporting Information is available free of charge on the ACS Publications website at DOI: 10.1021/acsami.5b02411.

AUTHOR INFORMATION

Corresponding Author

*E-mail: taihopark@postech.ac.kr. Fax: + 82-54-279-8298. Tel: 82-54-279-2394.

Notes

The authors declare no competing financial interest.

ACKNOWLEDGMENTS

This work was supported by grants from the Nano Material Technology Development Program (2012M3A7B4049989), Basic Science Research Program (NRF-2012M1A2A2671699), and the Center for Advanced Soft Electronics under the Global Frontier Research Program (Code No. NRF-2012M3A6A5055225) through the National Research Foundation of Korea (NRF) by the MSIP, Korea.

DOI: 10.1021/acsami.5b02411
ACS Appl. Mater. Interfaces 2015, 7, 11482−11489

REFERENCES

(1) Wang, D. H.; Kim, J. K.; Seo, J. H.; Park, I.; Hong, B. H.; Park, J. H.; Heeger, A. J. Transferable Graphene Oxide by Stamping Nanotechnology: Electron-Transport Layer for Efficient Bulk-Heterojunction Solar Cells. *Angew. Chem., Int. Ed.* **2013**, *52*, 2874−2880.

(2) He, Z.; Xiao, B.; Liu, F.; Wu, H.; Yang, Y.; Xiao, S.; Wang, C.; Russell, T. P.; Cao, Y. Single-Junction Polymer Solar Cells with High Efficiency and Photovoltage. *Nat. Photonics* **2015**, *9*, 174−179.

(3) Tsao, H. N.; Cho, D. M.; Park, I.; Hansen, M. R.; Mavrinskiy, A.; Yoon, D. Y.; Graf, R.; Pisula, W.; Spiess, H. W.; Müllen, K. Ultrahigh Mobility in Polymer Field-Effect Transistors by Design. *J. Am. Chem. Soc.* **2011**, *133*, 2605−2612.

(4) Kumar, A.; Lakhwani, G.; Elmalem, E.; Huck, W. T. S.; Rao, A.; Greenhama, N. C.; Friend, R. H. Interface Limited Charge Extraction and Recombination in Organic Photovoltaics. *Energy Environ. Sci.* **2014**, *7*, 2227−2231.

(5) Mazzio, K. A.; Luscombe, C. K. The Future of Organic Photovoltaics. *Chem. Soc. Rev.* **2015**, *44*, 78−90.

(6) Kim, H. G.; Kang, B.; Ko, H.; Lee, J.; Shin, J.; Cho, K. Synthetic Tailoring of Solid-State Order in Diketopyrrolopyrrole-Based Copolymers via Intramolecular Non-Covalent Interactions. *Chem. Mater.* **2015**, *27*, 829−838.

(7) Ye, L.; Zhang, S.; Zhao, W.; Yao, H.; Hou, J. Highly Efficient 2D-Conjugated Benzodithiophene-Based Photovoltaic Polymer with Linear Alkylthio Side Chain. *Chem. Mater.* **2014**, *26*, 3603−3605.

(8) Fu, Y.; Cha, H.; Lee, G. Y.; Moon, B. J.; Park, C. E.; Park, T. 3,6-Carbazole Incorporated into Poly[9,9-dioctylfluorene-alt-(bisthienyl)-benzothiadiazole]s Improving the Power Conversion Efficiency. *Macromolecules* **2012**, *45*, 3004−3009.

(9) Cha, H.; Lee, G. Y.; Fu, Y.; Park, C. E.; Park, T. Simultaneously Grasping and Self-Organizing Photoactive Polymers for Highly Reproducible Organic Solar Cells with Improved Efficiency. *Adv. Energy Mater.* **2013**, *3*, 1018−1024.

(10) Kim, H. I.; Trang, B. T. T.; Kim, G.-W.; Kang, G.; Shin, W. S.; Park, T. A. Benzodithiophene-Based Novel Electron Transport Layer for a Highly Efficient Polymer Solar Cell. *ACS Appl. Mater. Interfaces* **2014**, *6*, 15875−15880.

(11) Song, I. Y.; Kim, J.; Im, M. J.; Moon, B. J.; Park, T. Synthesis and Self-Assembly of Thiophene-Based All-Conjugated Amphiphilic Diblock Copolymers with a Narrow Molecular Weight Distribution. *Macromolecules* **2012**, *45*, 5058−5068.

(12) Moon, B. J.; Lee, G.-Y.; Im, M. J.; Song, S.; Park, T. In-Situ Modulation of the Vertical Distribution in a Blend of P3HT and $PC_{60}BM$ via the Addition of a Composition Gradient Inducer. *Nanoscale* **2014**, *6*, 2440−2446.

(13) Kim, J.; Song, I. Y.; Park, T. Polymeric Vesicles with a Hydrophobic Interior Formed by a Thiophene-Based All-Conjugated Amphiphilic Diblock Copolymer. *Chem. Commun.* **2011**, *47*, 4697−4699.

(14) Saito, Y.; Fukuri, N.; Senadeera, R.; Kitamura, T.; Wada, Y.; Yanagida, S. Solid State Dye Sensitized Solar Cells Using in Situ Polymerized PEDOTs as Hole Conductor. *Electrochem. Commun.* **2004**, *6*, 71−74.

(15) Saito, Y.; Azechi, T.; Kitamura, T.; Hasegawa, Y.; Wada, Y.; Yanagida, S. Photo-Sensitizing Ruthenium Complexes for Solid State Dye Solar Cells in Combination with Conducting Polymers as Hole Conductors. *Chem. Rev.* **2004**, *248*, 1469−1478.

(16) Xia, J.; Masaki, N.; Lira-Cantu, M.; Kim, Y.; Jiang, K.; Yanagida, S. Effect of Doping Anions' Structures on Poly(3,4-ethylenedioxythiophene) as Hole Conductors in Solid-State Dye-Sensitized Solar Cells. *J. Phys. Chem. C* **2008**, *112*, 11569−11574.

(17) Xia, J.; Masaki, N.; Lira-Cantu, M.; Kim, Y.; Jiang, K.; Yanagida, S. Influence of Doped Anions on Poly(3,4-ethylenedioxythiophene) as Hole Conductors for Iodine-Free Solid-State Dye-Sensitized Solar Cells. *J. Am. Chem. Soc.* **2008**, *130*, 1258−1263.

(18) Liu, X.; Zhang, W.; Uchida, S.; Cai, L.; Liu, B.; Ramakrishna, S. An Efficient Organic-Dye-Sensitized Solar Cell with In Situ Polymerized Poly(3,4-ethylenedioxythiophene) as a Hole-Transporting Material. *Adv. Mater.* **2010**, *22*, E150−E155.

(19) Zhang, J.; Yang, L.; Shen, Y.; Park, B.-W.; Hao, Y.; Johansson, E. M. J.; Boschloo, G.; Kloo, L.; Gabrielsson, E.; Sun, L.; Jarboui, A.; Perruchot, C.; Jouini, M.; Vlachopoulos, N.; Hagfeldt, A. Poly(3,4-ethylenedioxythiophene) Hole-Transporting Material Generated by Photoelectrochemical Polymerization in Aqueous and Organic Medium for All-Solid-State Dye-Sensitized Solar Cells. *J. Phys. Chem. C* **2014**, *118*, 16591−16601.

(20) Yang, L.; Zhang, J.; Shen, Y.; Park, B.-W.; Bi, D.; Häggman, L.; Johansson, E. M. J.; Boschloo, G.; Hagfeldt, A.; Vlachopoulos, N.; Snedden, A.; Kloo, L.; Jarboui, A.; Chams, A.; Perruchot, C.; Jouini, M. New Approach for Preparation of Efficient Solid-State Dye-Sensitized Solar Cells by Photoelectrochemical Polymerization in Aqueous Micellar Solution. *J. Phys. Chem. Lett.* **2013**, *4*, 4026−4031.

(21) Liu, X.; Cheng, Y.; Wang, L.; Caia, L.; Liu, B. Light Controlled Assembling of Iodine-Free Dye-sensitized Solar Cells with Poly(3,4-ethylenedioxythiophene) as a Hole Conductor reaching 7.1% Efficiency. *Phys. Chem. Chem. Phys.* **2012**, *14*, 7098−7013.

(22) Lee, W.; Roh, S.-J.; Hyung, K.-H.; Park, J.; Lee, S.-H.; Han, S.-H. Photoelectrochemically Polymerized Polythiophene Layers on Ruthenium Photosensitizers in Dye-Sensitized Solar Cells and their Beneficial Effects. *Sol. Energy* **2009**, *83*, 690−695.

(23) Song, I. Y.; Park, S.-H.; Lim, J.; Kwon, Y. S.; Park, T. A Novel Hole Transport Material for Iodine-Free Solid State Dye-Sensitized Solar Cells. *Chem. Commun.* **2011**, *47*, 10395−10397.

(24) Song, I. Y.; Kwon, Y. S.; Lim, J.; Park, T. Well-Defined All-Conducting Block Copolymer Bilayer Hybrid Nanostructure: Selective Positioning of Lithium Ions and Efficient Charge Collection. *ACS Nano* **2014**, *8*, 6893−6901.

(25) Hirata, N.; Kroeze, J. E.; Park, T.; Jones, D.; Haque, S. A.; Holmes, A. B.; Durrant, J. R. Interface Engineering for Solid-State Dye-Sensitised Nanocrystalline Solar Cells: The Use of an Organic Redox Cascade. *Chem. Commun.* **2006**, 535−537.

(26) Haque, S. A.; Park, T.; Xu, C.; Koops, S.; Schulte, N.; Potter, R. J.; Holmes, A. B.; Durrant, J. R. Interface Engineering for Solid-State Dye-Sensitized Nanocrystalline Solar Cells: The Use of Ion-Solvating Hole-Transporting Polymers. *Adv. Funct. Mater.* **2004**, *14*, 435−440.

(27) Dolan, A. R.; Wood, T. D. Analysis of Polyaniline Oligomers by Laser Desorption Ionization and Solvent-less MALDI. *J. Am. Soc. Mass. Spectrom.* **2004**, *15*, 893−899.

(28) Park, T.; Zimmerman, S. C.; Nakashima, S. A Highly Stable Quadruply Hydrogen-Bonded Heterocomplex Useful for Supramolecular Polymer Blends. *J. Am. Chem. Soc.* **2005**, *127*, 6520−6521.

(29) Abate, A.; Hollman, D. J.; Teuscher, J.; Pathak, S.; Avolio, R.; D'Errico, G.; Vitiello, G.; Fantacci, S.; Snaith, H. J. Protic Ionic Liquids as *p*-Dopant for Organic Hole Transporting Materials and Their Application in High Efficiency Hybrid Solar Cells. *J. Am. Chem. Soc.* **2013**, *135*, 13538−13548.

(30) Lu, S.; Lepore, S. D.; Li, S. Y.; Mondal, D.; Cohn, P. C.; Bhunia, A. K.; Pike, V. W. Nucleophile Assisting Leaving Groups: A Strategy for Aliphatic ^{18}F-Fluorination. *J. Org. Chem.* **2009**, *74*, 5290−5296.

(31) Thordarson, P. Determining Association Constants from Titration Experiments in Supramolecular Chemistry. *Chem. Soc. Rev.* **2011**, *40*, 1305−1323.

(32) Kim, J.; Kwon, Y. S.; Shin, W. S.; Moon, S.-J.; Park, T. Carbazole-Based Copolymers: Effects of Conjugation Breaks and Steric Hindrance. *Macromolecules* **2011**, *44*, 1909−1919.

(33) Yanagida, S.; Yu, Y.; Manseki, K. Iodine/Iodide-Free Dye-Sensitized Solar Cells. *Acc. Chem. Res.* **2009**, *42*, 1827−1838.

(34) Tachibana, Y.; Haque, S. A.; Mercer, I. P.; Moser, J. E.; Klug, D. R.; Durrant, J. R. Modulation of the Rate of Electron Injection in Dye-Sensitized Nanocrystalline TiO_2 Films by Externally Applied Bias. *J. Phys. Chem. B* **2001**, *105*, 7424−7431.

(35) Koops, S. E.; O'Regan, B. C.; Barnes, P. R. F.; Durrant, J. R. Parameters Influencing the Efficiency of Electron Injection in Dye-Sensitized Solar Cells. *J. Am. Chem. Soc.* **2009**, *131*, 4808−4818.

(36) Melas-Kyriazi, J.; Ding, I.-K.; Marchioro, A.; Punzi, A.; Hardin, B. E.; Burkhard, G. F.; Tétreault, N.; Grätzel, M.; Moser, J.-E.; McGehee, M. D. The Effect of Hole Transport Material Pore Filling

DOI: 10.1021/acsami.5b02411
ACS Appl. Mater. Interfaces 2015, 7, 11482−11489

on Photovoltaic Performance in Solid-State Dye-Sensitized Solar Cells. *Adv. Energy Mater.* **2011**, *1*, 407−414.
(37) Kwon, Y. S.; Lim, J.; Yun, H.; Kim, Y.; Park, T. A Diketopyrrolopyrrole-Containing Hole Transporting Conjugated Polymer for Use in Efficient Stable Organic-Inorganic Hybrid Solar Cells Based on a Perovskite. *Energy Environ. Sci.* **2014**, *7*, 1454−1460.
(38) Kley, C. S.; Dette, C.; Rinke, G.; Patrick, C. E.; Cechal, J.; Jung, S. J.; Baur, M.; Durr, M.; Rauschenbach, S.; Giustino, F.; Stepanow, S.; Kern, K. Atomic-Scale Observation of Multiconformational Binding and Energy Level Alignment of Ruthenium-based Photosensitizers on TiO_2 Anatase. *Nano Lett.* **2014**, *14*, 563−569.
(39) Lim, J.; Kim, T.; Park, T. Fast Cascade Neutralization of an Oxidized Sensitizer by an In Situ-Generated Ionic Layer of I^- Species on a Nanocrystalline TiO_2 Electrode. *Energy Environ. Sci.* **2014**, *7*, 4029−4034.
(40) Cahen, D.; Hodes, G.; Grätzel, M.; Guillemoles, J.; Riess, I. Nature of Photovoltaic Action in Dye-Sensitized Solar Cells. *J. Phys. Chem. B* **2000**, *104*, 2053−2059.
(41) Schlichthorl, G.; Park, N. G.; Frank, A. J. Evaluation of the Charge-Collection Efficiency of Dye-Sensitized Nanocrystalline TiO_2 Solar Cells. *J. Phys. Chem. B* **1999**, *103*, 782−791.
(42) Hagfeldt, A.; Grätzel, M. Molecular Photovoltaics. *Acc. Chem. Res.* **2000**, *33*, 269−277.
(43) Lim, J.; Kwon, Y. S.; Park, T. Effect of Coadsorbent Properties on the Photovoltaic Performance of Dye-Sensitized Solar Cells. *Chem. Commun.* **2011**, *47*, 4147−4149.
(44) Boschloo, G.; Hagfeldt, A. Characteristics of the Iodide/Triiodide Redox Mediator in Dye-Sensitized Solar Cells. *Acc. Chem. Res.* **2009**, *42*, 1819−1826.
(45) Park, S.; Lim, J.; Kwon, Y. S.; Song, I. Y.; Choi, J. M.; Song, S.; Park, T. Tunable Nanoporous Network Polymer Nanocomposites having Size-Selective Ion Transfer for Dye-Sensitized Solar Cells. *Adv. Energy Mater.* **2013**, *3*, 184−192.
(46) Park, S. H.; Song, I. Y.; Lim, J.; Kwon, Y. S.; Choi, J.; Song, S.; Lee, J.-R.; Park, T. A Novel Quasi-Solid State Dye-Sensitized Solar Cell Fabricated Using a Multifunctional Network Polymer Membrane Electrolyte. *Energy Environ. Sci.* **2013**, *6*, 1559−1564.
(47) Kuang, D.; Wang, P.; Ito, S.; Zakeeruddin, S. M.; Grätzel, M. Stable Mesoscopic Dye-Sensitized Solar Cells Based on Tetracyanoborate Ionic Liquid Electrolyte. *J. Am. Chem. Soc.* **2006**, *128*, 7732−7733.
(48) Choi, J.; Song, S.; Kang, G.; Park, T. Dye-Sensitized Solar Cells Employing Doubly or Singly Open-Ended TiO_2 Nanotube Arrays: Structural Geometry and Charge Transport. *ACS Appl. Mater. Interfaces* **2014**, *6*, 15388−15394.
(49) Venkateswararao, A.; Thomas, K. R. J.; Li, C.-T.; Ho, K.-C. Functional Tuning of Organic Dyes Containing 2,7-Carbazole and other Electron-Rich Segments in the Conjugation Pathway. *RSC Adv.* **2015**, *5*, 17953−17966.
(50) Park, S.-H.; Lim, J.; Song, I. Y.; Lee, J.-R.; Park, T. Physically Stable Polymer-Membrane Electrolytes for Highly Efficient Solid-State Dye-Sensitized Solar Cells with Long-Term Stability. *Adv. Energy Mater.* **2014**, *4*, 1300489−1300495.
(51) Zhu, K.; Neale, N. R.; Miedaner, A.; Frank, A. J. Enhanced Charge-Collection Efficiencies and Light Scattering in Dye-Sensitized Solar Cells Using Oriented TiO_2 Nanotubes Arrays. *Nano Lett.* **2007**, *7*, 69−74.
(52) Choi, J.; Park, S.-H.; Kwon, Y. S.; Lim, J.; Song, I. Y.; Park, T. Facile Fabrication of Aligned Doubly Open-Ended TiO_2 Nanotubes, via a Selective Etching Process, for Use in Front-Illuminated Dye Sensitized Solar Cells. *Chem. Commun.* **2012**, *48*, 8748−8750.
(53) Choi, J.; Kwon, Y. S.; Park, T. Doubly Open-Ended TiO_2 Nanotube Arrays Decorated with a Few nm-Sized TiO_2 Nanoparticles for Highly Efficient Dye-Sensitized Solar Cells. *J. Mater. Chem. A* **2014**, *2*, 14380−14385.
(54) Choi, J.; Kang, G.; Park, T. A Competitive Electron Transport Mechanism in Hierarchical Homogeneous Hybrid Structures Composed of TiO_2 Nanoparticles and Nanotubes. *Chem. Mater.* **2015**, *27*, 1359−1366.
(55) Kuang, D.; Klein, C.; Snaith, H. J.; Moser, J.-E.; Humphry-Baker, R.; Comte, P.; Zakeeruddin, S. M.; Grätzel, M. Ion Coordinating Sensitizer for High Efficiency Mesoscopic Dye-Sensitized Solar Cells: Influence of Lithium Ions on the Photovoltaic Performance of Liquid and Solid-State Cells. *Nano Lett.* **2006**, *6*, 769−773.

DOI: 10.1021/acsami.5b02411
ACS Appl. Mater. Interfaces 2015, 7, 11482−11489